CAUSTIC INSOLUBLE ALUMINIUM CONTAINING NANOMINERALS IN BAUXITE FROM SOUTH WESTERN AUSTRALIA

Robert Gilkes[1], Saowanuch Tawornpruek[2], Nattaporn Prakongkep[1], Colin Scanlan[3], Wayne Tichbon[3], Alex Aboagye[3]

[1] School of Earth and Environment, Faculty of Natural and Agricultural Sciences, University of Western Australia, Crawley, WA 6009, Australia

[2] Department of Soil Science, Faculty of Agriculture, Kasetsart University, Bangkok 10900, Thailand

[3] BHP Billiton Worsley Alumina Pty Ltd PO Box 344 Collie WA 6225, Australia

Abstract

Conventional and synchrotron XRD show that gibbsite, hercynite, corundum, poorly ordered aluminas, boehmite, goethite, hematite, maghemite, muscovite, kaolinite, anatase, quartz, and rutile are present in WA Darling Range bauxite. A significant proportion of the Al in this bauxite is not dissolved by Bayer liquor. We have concentrated various aluminas, hercynite, iron oxides, kaolin and muscovite in the caustic insoluble residue and characterized these minerals using conventional and synchrotron X-ray diffraction and high resolution analytical electron microscopy (EDS, EELS, SAD, HRTEM).

Caustic soluble gibbsite [$Al(OH)_3$] is the major aluminium mineral in these bauxites however the presence of caustic insoluble Al in nanometric corundum, hercynite, iron oxides, poorly ordered aluminas, and muscovite may substantially reduce aluminium extraction from some bauxite.

1. Introduction

Boddington bauxite from the Darling Range lateritic bauxite province in south-western Australia has formed from diverse granitic and mafic parent rocks. The bauxite profile contains saprock, saprolite, pallid clay, B-zone ore, hardcaps and gravel [1]. The mined bauxite represents a mixture of B-zone, hardcap and gravel with a mineralogy dominated by gibbsite, goethite, hematite and quartz. Minor constituents include boehmite, corundum, maghemite, anatase, kaolin and muscovite together with diverse resistant sand-size primary mineral grains (zircon, monazite, etc).

Extraction of Al from this bauxite using the Bayer process varies in efficiency with the type of bauxite being processed and in particular with the mineralogy of the bauxite. This paper identifies forms of Al that are not dissolved during Bayer process extraction and which are responsible for differences in extraction efficiency between bauxite materials.

2. Materials and Methods

Samples of gravel, caprock and B-grade bauxite from the Boddington mine and residues of these materials after caustic digestion were examined. Caustic digestion treatment removed gibbsite and kaolinite and concentrated iron oxides and other minerals. Iron oxides were removed from the samples by DCB (dithionite-citrate-bicarbonate) treatment [2,3]. Maghemite was separated by magnetic separation (MAG) and quartz was removed from the concentrates by sedimentation and sometimes heavy liquid separation.

For random powder X-ray diffraction (XRD) measurements, mineral concentrate samples were scanned from 4 to 65° 2θ, using a step size of 0.02° 2θ and a scan speed of 0.004° 2θ sec^{-1} [4] with a Philips PW-3020 diffractometer using CuKα radiation and a graphite monochromator.

XRD patterns of the mineral concentrate samples were also obtained using synchrotron radiation on the Australian synchrotron. Powdered mineral concentrate samples were placed in glass capillaries, and analyzed over an angular range of 4–60° 2θ. The wavelength was set at ~0.1 nm to provide for adequate dispersion/resolution.

The TEM specimens were prepared using the clay fraction which was ultrasonically dispersed in ultrapure water and a few drops of the suspension were deposited on a copper grid covered with a holey carbon film. TEM-EDS (transmission electron microscopy with energy dispersive analysis of X-rays), EFTEM (energy filtered transmission electron microscopy), SAD (selected area diffraction) and high resolution transmission electron microscopy (HRTEM) data for particles were obtained with a JEOL 3000F FEGTEM operated at 300 kV to determine the morphology and composition of mostly submicron size particles. A 300 kV JEOL 3000F field-emission TEM equipped with a post-column Gatan Imaging Filter, a TV-rate retractable camera and Multi Scan digital camera (Gatan, Pleasanton, CA) was employed for EFTEM work.

3. Results

Figure 1 shows the Al_2O_3 concentrations in various bauxite materials and residues after digestion in raw caustic and Bayer liquor. It is evident that for some materials a high proportion of Al_2O_3 was not dissolved in either raw caustic or Bayer liquor. Even for those samples where most Al_2O_3 was dissolved there was a significant amount of Al_2O_3 in the residues with this amount being greater for Bayer liquor residue. The research described below is focused on the identification of Al-containing minerals in these insoluble residues.

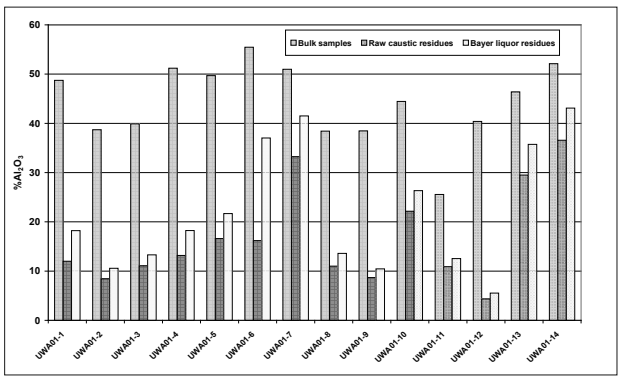

Figure 1. %Al2O3 in bulk samples and caustic digest residues, determined by XRF.

3.1 Mineralogy of caustic insoluble residues

XRD patterns of a gravel and residues after digestion in raw caustic and Bayer liquor are shown in Figure 2. Semi-quantitative estimates of mineralogy derived from XRD data are indicated in this figure.

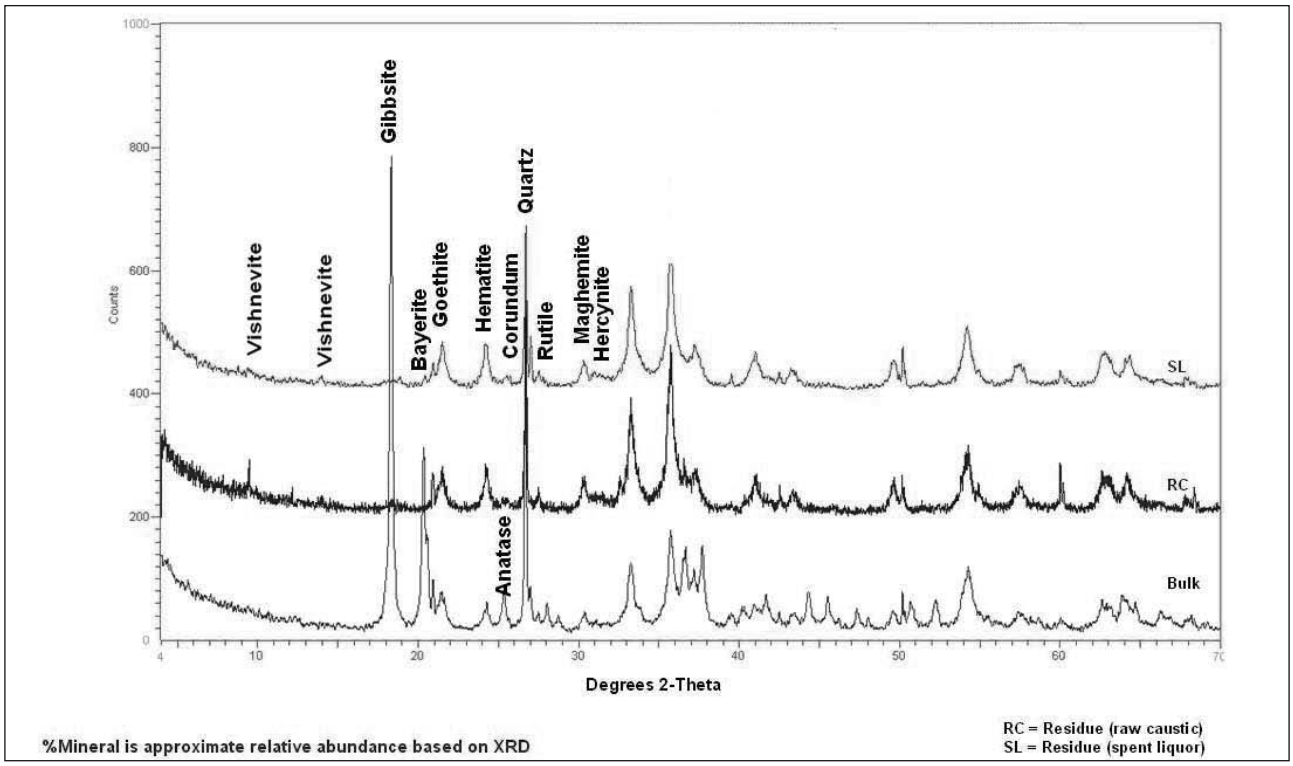

Figure 2. XRD patterns of UWA01-10 bauxite bulk sample and residues, with inset tables showing calculated %minerals and %Al in minerals. Please note that the XRD technique does not give highly accurate or precise measures of abundance or composition so the data in the table are approximate.

Gibbsite ($Al(OH_3)$) almost completely dissolved and vishnevite and bayerite precipitated during the caustic digest procedure. Some of the bayerite has precipitated during incomplete washing of the caustic digest residue. Eight caustic-insoluble accessory minerals were concentrated by the digests and of these goethite, hematite, corundum and hercynite contain structural Al. Thus we have identified at least some of the forms of caustic-insoluble Al in this bauxite. Amounts of Al in these minerals are shown in Figure 2. Bauxite caustic residues may also contain muscovite which contains structural Al, and minor feldspar may also be present. The estimate of amounts of Al present in caustic insoluble minerals is based on analyses of these samples by XRD.

Gibbsite occurs as subhedral to euhedral hexagonal crystals ranging in size from 0.1-1 µm (Figure 3). Gibbsite contains little or no substitution of Fe or other elements. Corundum (α-Al_2O_3) may represent up to 30% of gravelly bauxite and consists of 20-200 nm anhedral to subhedral platey crystals, often with a distinct granular texture [8]. These particles are not aggregates but single crystals as is demonstrated by extensive continuous lattice images throughout particles and associated single crystal diffraction patterns (Figure 4).

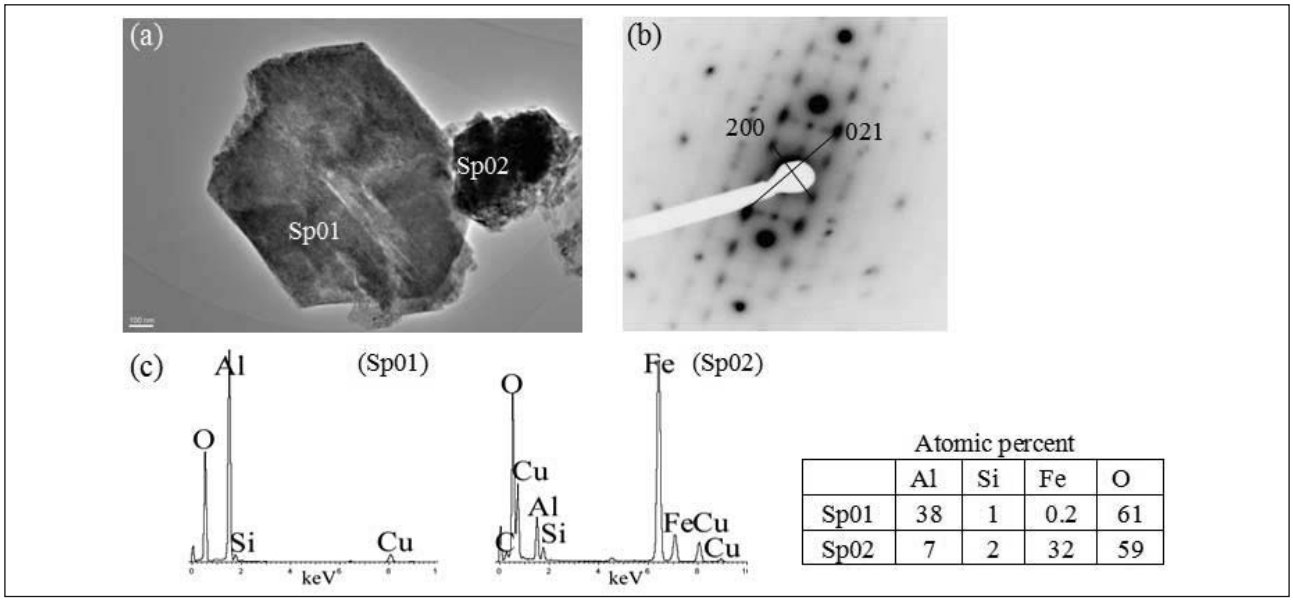

Atomic percent

	Al	Si	Fe	O
Sp01	38	1	0.2	61
Sp02	7	2	32	59

Figure 3. (a) Electron micrograph of gibbsite (Sp01) and aluminous goethite (Sp02) particles, (b) electron diffraction pattern of the gibbsite particle (Sp01) and (c) x-ray spectra of the gibbsite particle (Sp01) and the aluminous goethite particle (Sp02) (The Si and Cu peaks are due to supporting film and grid respectively).

Minor amounts of Fe^{3+} are generally associated with corundum crystals as indicated by energy filtered electron micrographs and associated EELS spectra (Figure 5). This minor amount of Fe^{3+} (about 1 atom %) is not uniformly distributed throughout crystals and may consist of Fe-oxide particles on the surface and in voids in corundum particles. However the particles shown in Figures 4 and 5 had been extracted with citrate-bicarbonate-dithionite solution to remove free iron oxides so that the Fe indicated by these data is more likely present within the structure of corundum. Such low amounts of Fe substitution did not affect unit cell dimensions.

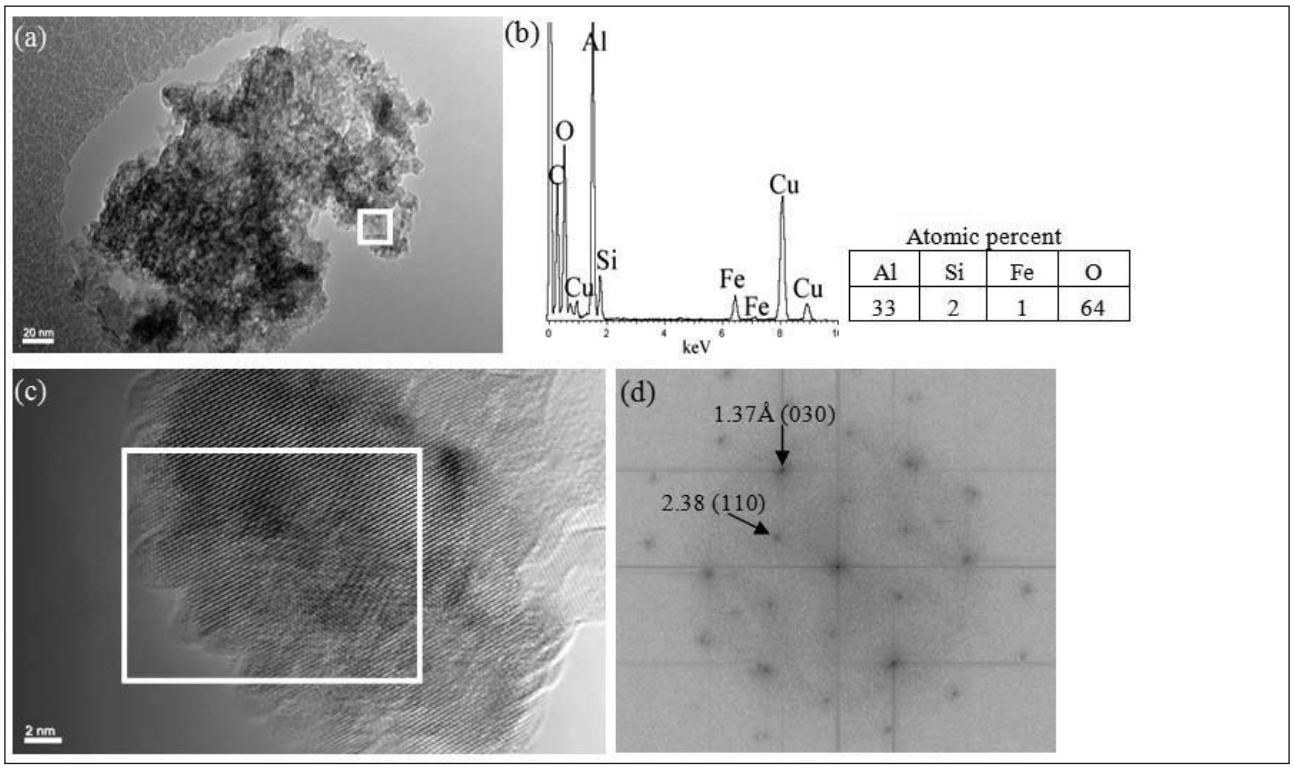

Figure 4. (a) Electron micrograph of a corundum particle, (b) x-ray spectrum of the particle indicating minor substitution of Fe for Al (The Si and Cu peaks are due to the supporting film and grid respectively), (c) high resolution electron micrograph of the area indicated by the white square in (a) and (d) Fourier transform diffraction pattern of a region of the corundum particle indicated by the white square in (c).

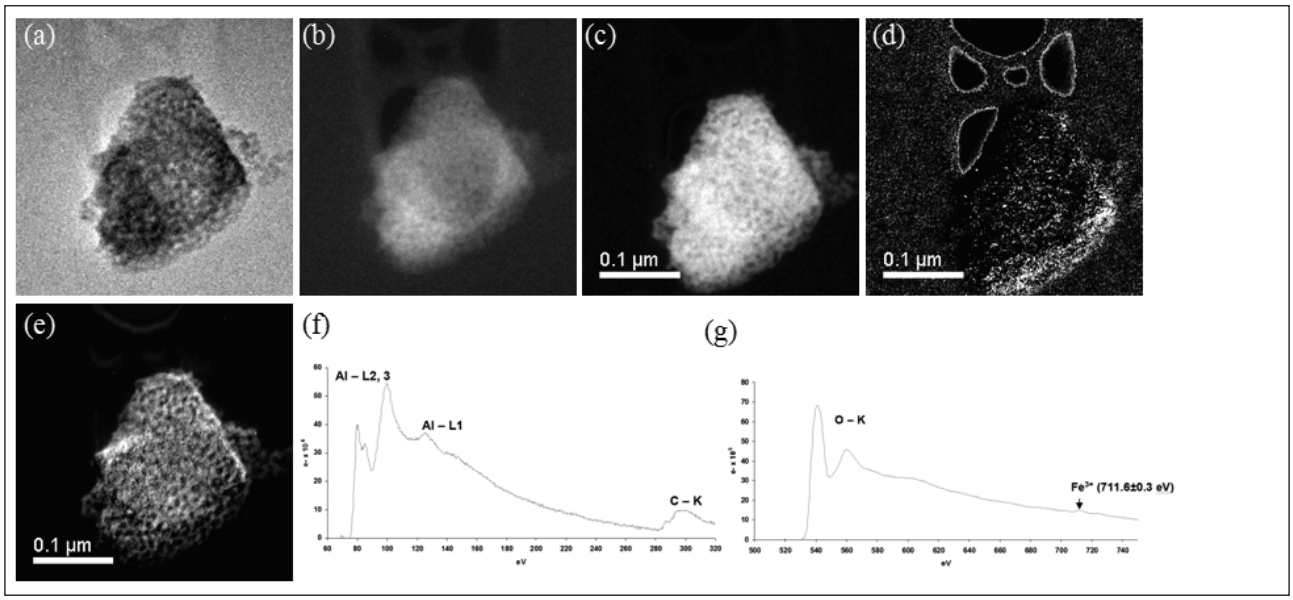

Figure 5. (a) Energy filtered electron micrograph of a corundum particle, (b) thickness map, (c) oxygen map, (d) iron map, (e) aluminium map, (f) EELS for aluminium and carbon, (g) EELS for oxygen and ferric iron.

3.2 Hercynite.

Hercynite (ideally Al_2FeO_4 – Fe present as Fe^{2+}) was mostly present in gravel and hardcap materials and was never present at amounts greater than 10%. It consists of anhedral granular platey 20-200 nm particles with lattice fringes extending throughout particles that generate Fourier transform diffraction patterns thus indicating that the particles are single crystals (Figure 6). X-ray spectra of hercynite particles indicate that the composition is quite variable and particles often contain more Al than ideal hercynite. EELS spectra show that Fe is present as Fe^{2+} (Figure 7).

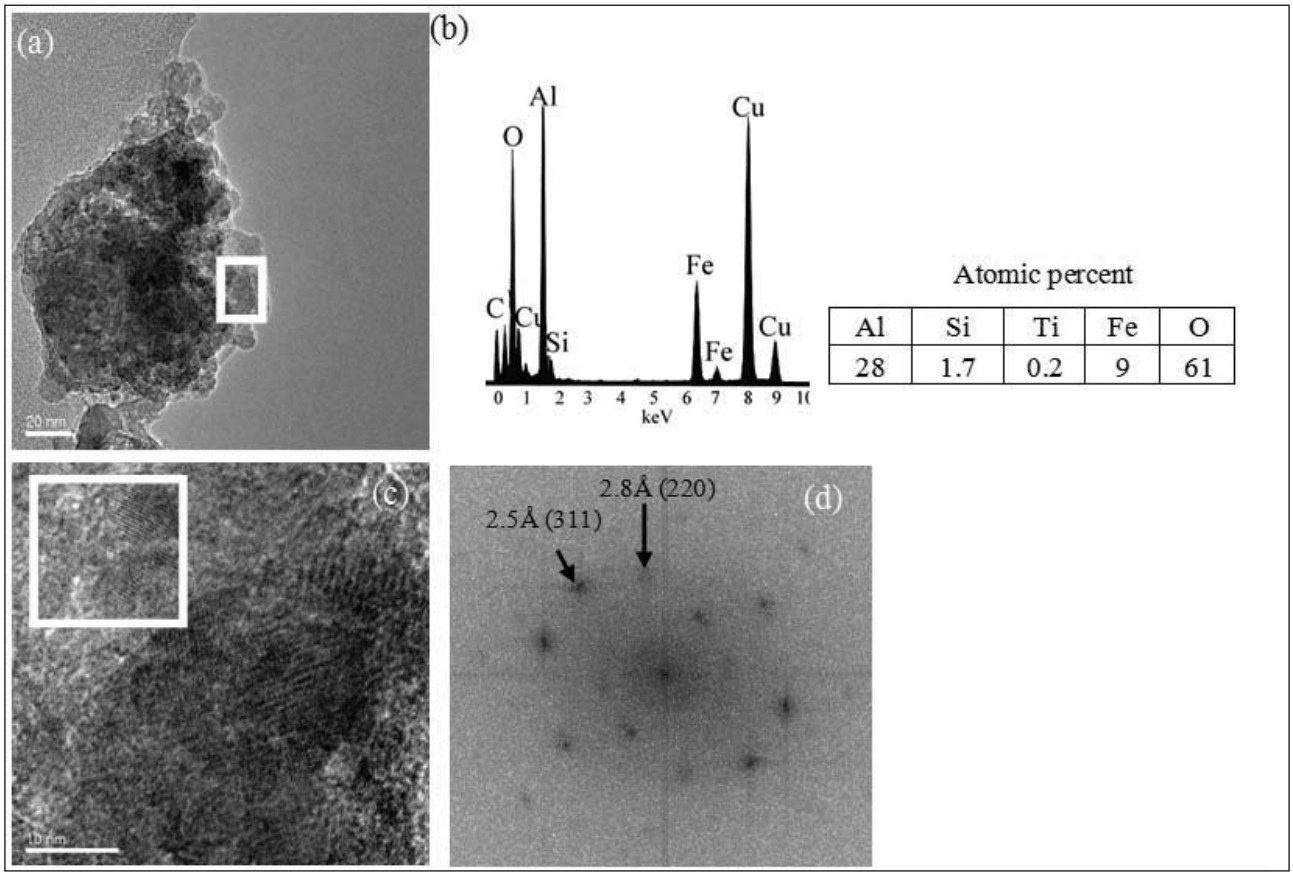

Figure 6. (a) Electron micrograph of a hercynite particle, (b) x-ray spectrum of the particle (The Si and Cu peaks are due to the supporting film and grid respectively), (c) high resolution electron micrograph of the indicated area of the particle showing a lattice image and (d) Fourier transform diffraction pattern for the indicated area in (c).

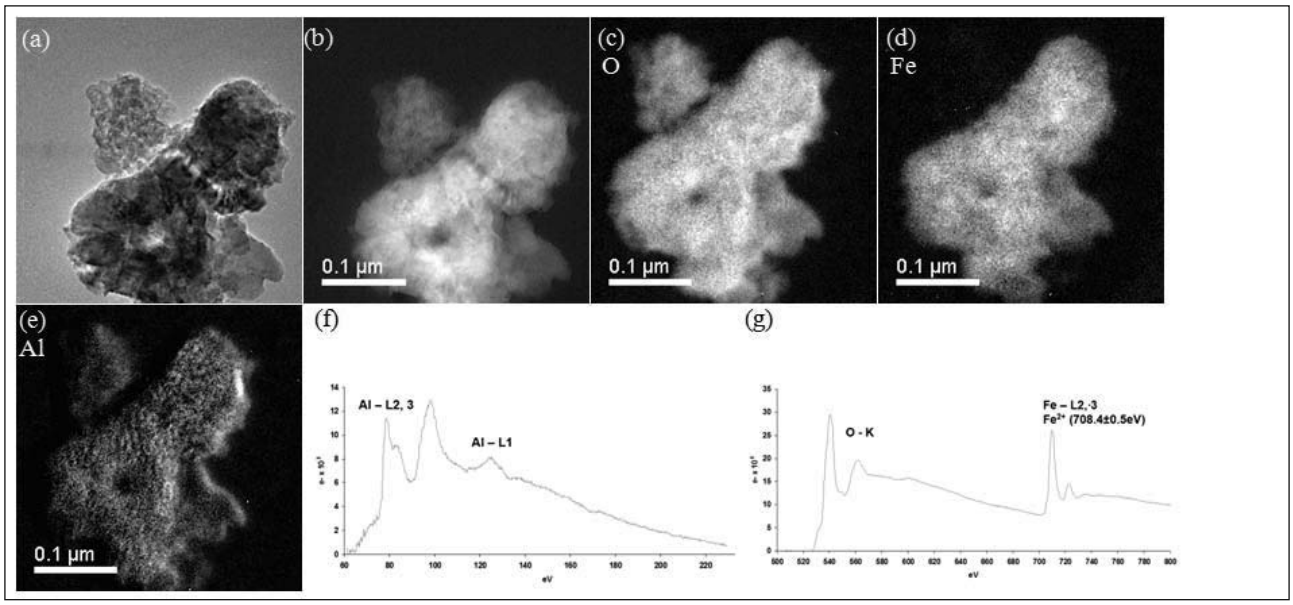

Figure 7. (a) Energy filtered electron micrographs of the hercynite particles, (b) thickness map, (c) oxygen map, (d) iron map, (e) aluminium map, (f) EELS for aluminium and (g) EELS for oxygen and iron which corresponds to ferrous (Fe2+).

3.3 Goethite.

Goethite (α FeOOH) in bauxite contains high levels of Al substitution (Figures 3 and 8) and most of this structural Al is not dissolved during caustic extraction. Goethite particles are 20-2000 nm platey anhedral with a granular appearance as if they are composed of many nanometric subcrystals. Some particles give extensive lattice images indicating that some plates are single crystals resting on their (001) face but often lattice images do not extend throughout the entire volume of particles which may therefore be aggregates of two or more crystals (Figure 8g).

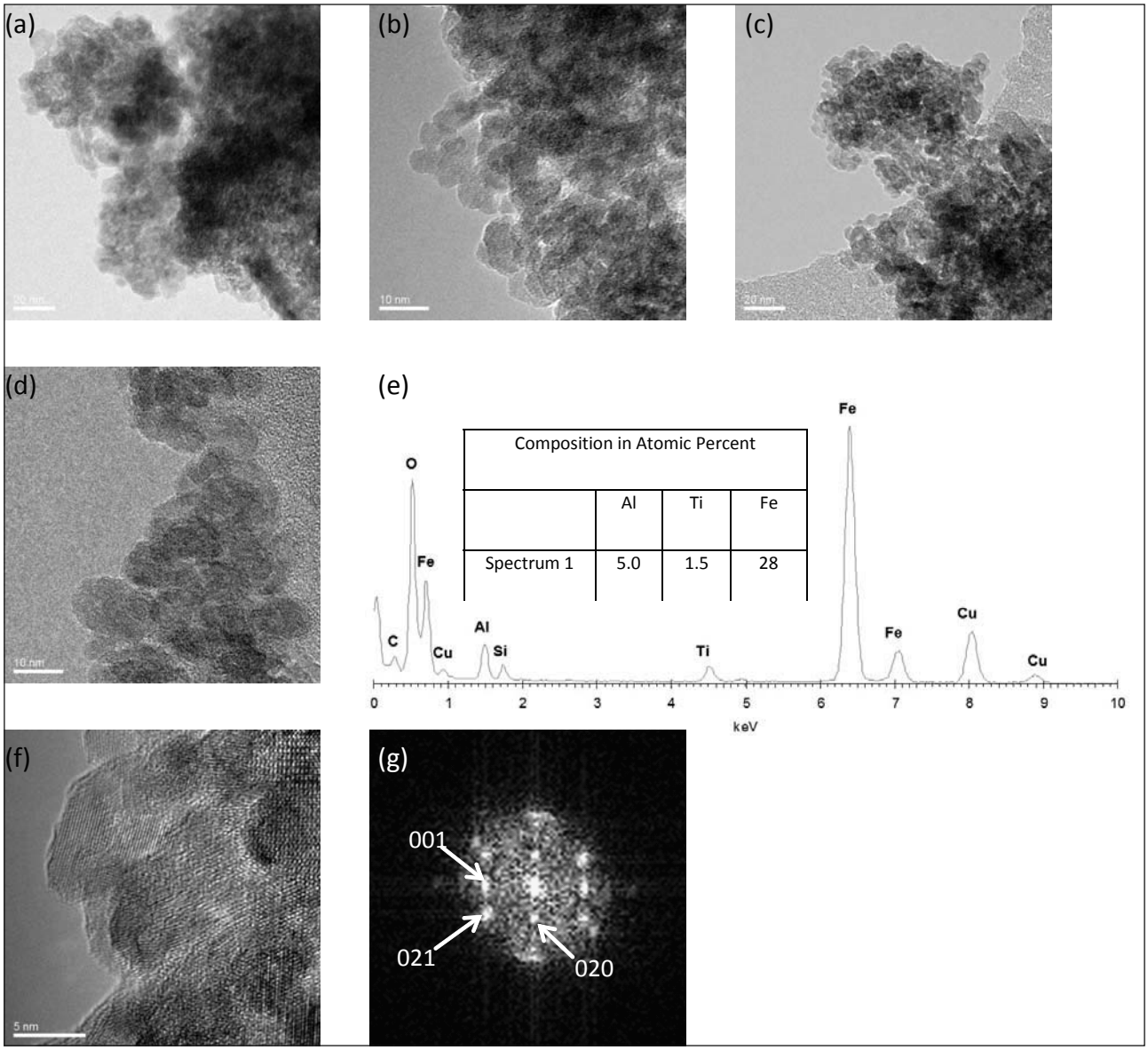

Figure 8. **(a, b, c, and d) Electron micrographs of goethite particles from the goethite concentrate sample indicating that the particles consist of aggregates of anhedral subhedral platy 7-15 nm crystals, (e) eds spectrum of (d) and analyses of 5 particles indicating extensive Al and possible minor Ti substitution for Fe, (f) High resolution electron micrograph and (g) Fourier transform diffraction pattern of a goethite particle. The lattice images throughout the particle are not continuous through subgrains possibly indicating that the particle is not a single crystal.**

3.4 Hematite.

Hematite (α Fe_2O_3) crystals are similar to those of goethite being anhedral and granular in appearance with plates being perpendicular to the c-axis (Figure 9). Levels of Al-substitution for Fe in hematite are mostly much smaller than for goethite; however a wide range of Al substitution levels exists.

3.5 Maghemite.

Maghemite (γ-Fe_2O_3) crystals resemble crystals of goethite and hematite being 50-200 nm, anhedral and platey but they mostly do not have a granular fabric (Figure 10). EDS data indicate that minor Al substitution may occur. EELS spectra indicate that Fe is present as Fe^{3+} in maghemite (Figure 10).

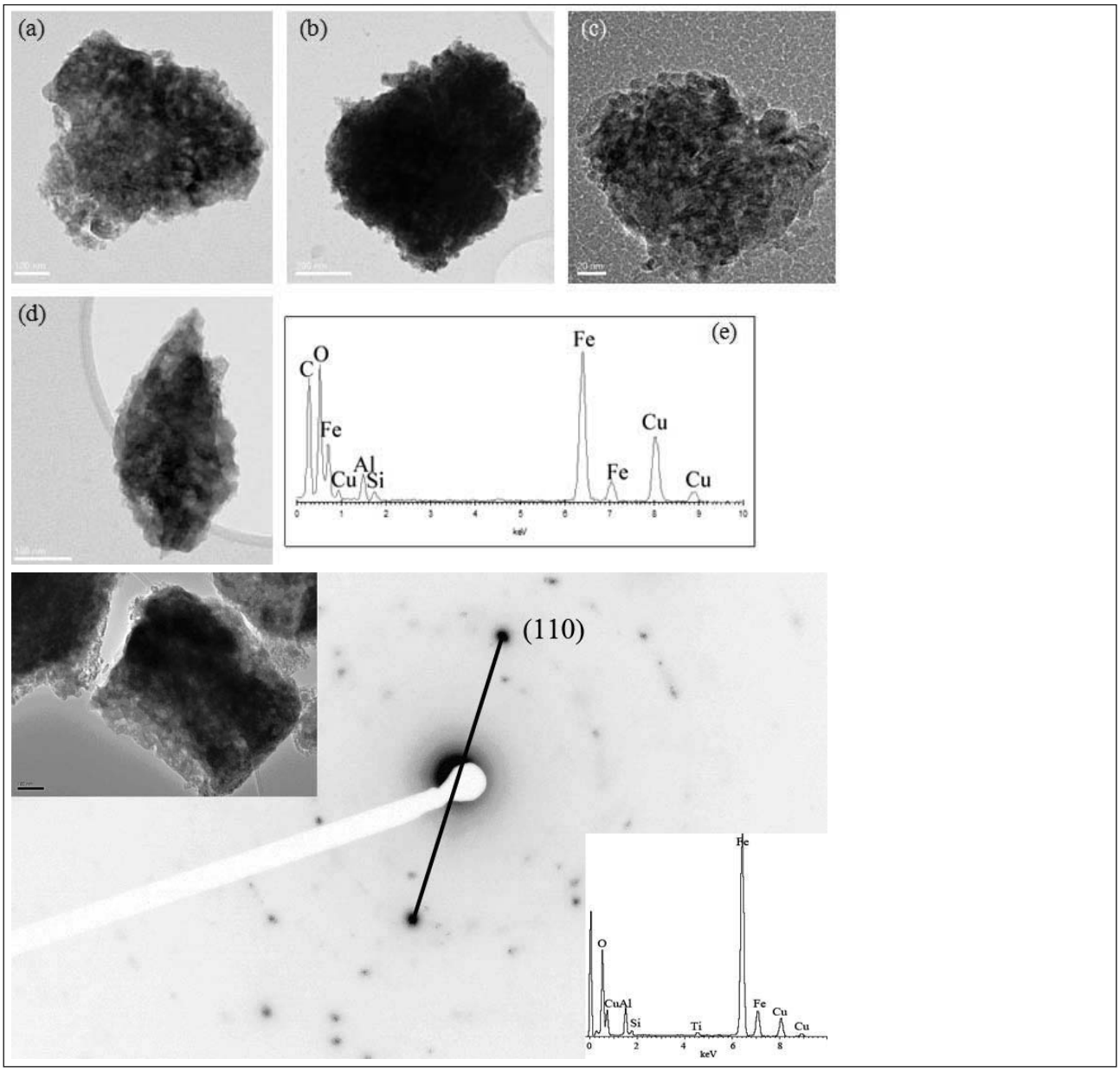

Figure 9. Electron micrographs of hematite particles (a, b, c, d) showing that particles are complex aggregates of ~20 nm platey subcrystals (e) EDS spectrum of the particle shown in (b) indicating substantial Al substitution for Fe. The Si and Cu peaks are due to the supporting film and grid respectively.The crystal of Al-rich hematite shown at the bottom of the figure is resting on its (001) face as indicated by the electron diffraction pattern.

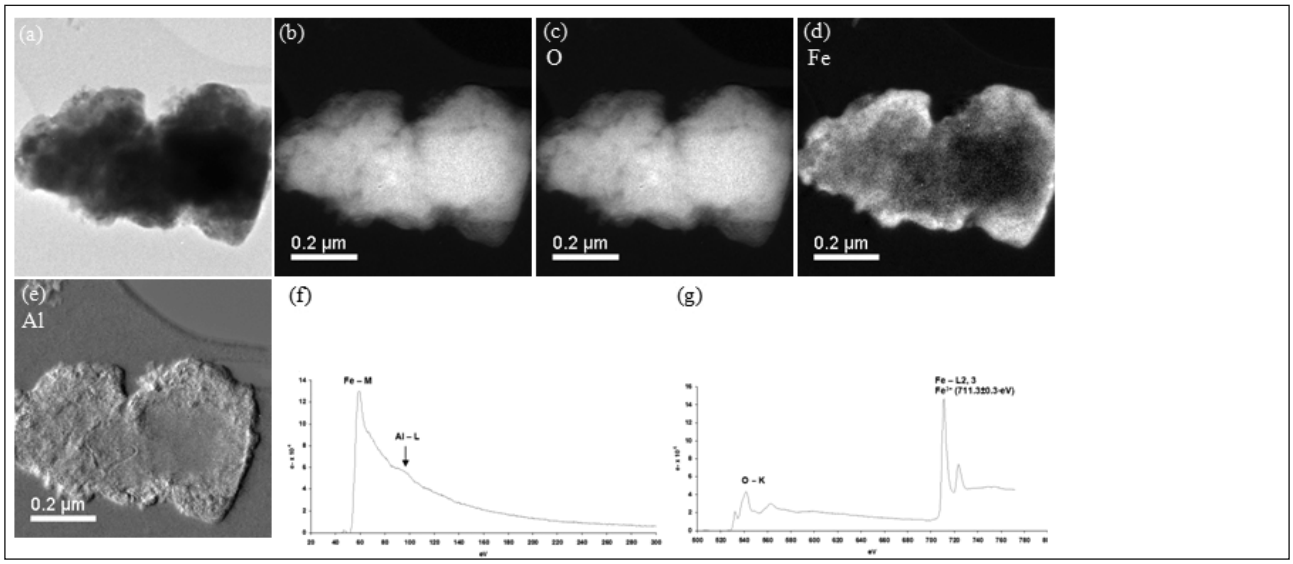

Figure 10. (a) Energy filtered electron micrograph of part of a maghemite particle, (b) thickness map, (c) oxygen map, (d) iron map, (e) aluminium map, (f) EELS for iron and aluminium, (g) EELS for oxygen and iron (ferric Fe^{3+}).

3.6 Muscovite.

Silt-size fragments of muscovite occur in bauxite (Figure 11) and are not dissolved by caustic extraction although the potassium content is usually much smaller than in ideal muscovite which may be partly due to Na in caustic replacing some K.

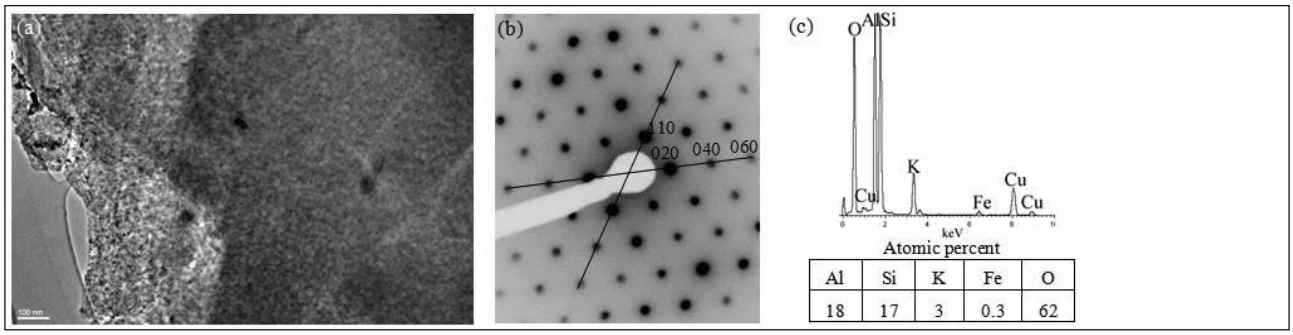

Al	Si	K	Fe	O
18	17	3	0.3	62

Figure 11. (a) Electron micrograph of a muscovite particle, (b) electron diffraction pattern of (a) the particle and (c) x-ray spectrum of the particle (The Cu peaks are due to the supporting grid).

3.7 Kaolin.

Kaolin is a minor constituent of bauxite and especially of caustic residue as it is highly soluble at high pH. It may however be protected in iron oxide aggregates as with the example in Figure 12 which shows kaolinite in the residue of the caustic digest of maghemite-rich bauxite gravel. Kaolin occurs as subhedral to euhedral crystals and EDS spectra indicate that it may contain minor substitution of Fe for Al as has been reported by [6] (Figure 12).

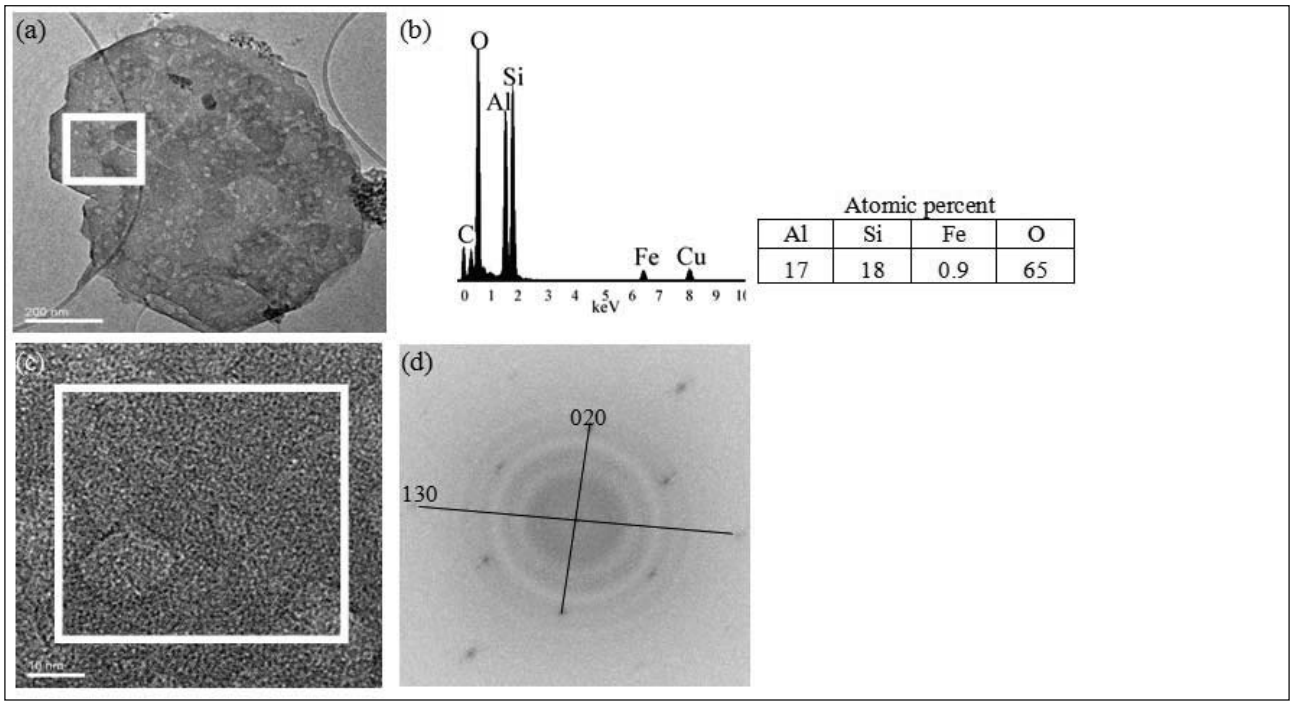

Al	Si	Fe	O
17	18	0.9	65

Figure 12. (a) Electron micrograph of a kaolin particle, (b) x-ray spectrum of the particle (The Cu peaks are due to the supporting grid), (c) high resolution electron micrograph of the area within the white square in (a) and (d) Fourier transform diffraction pattern of the region of the kaolin particle indicated by a white square area in (c).

3.8 Poorly Ordered Aluminas.

XRD patterns of caustic residues of some gravel and hardcap samples indicate that poorly ordered gamma and chi aluminas are present in bauxite. These minerals are not dissolved by the Bayer process.

4. Conclusion

This XRD and electron optical examination of residues of caustic and other extractions of diverse bauxite materials from the Boddington bauxite deposit has identified several Al-containing minerals that comprise the non-available Al in this deposit. This knowledge is valuable to the development of improved ore evaluation and Al extraction procedures.

5. Acknowledgments

We are grateful to BHP Billiton Worsley Alumina Pty Ltd for providing financial assistance to carry out this work and special thanks to Professor Martin Saunders, Centre of Microscopy, Characterisation and Analysis, The University of Western Australia for their excellent TEM technique support. We thank the Australian Synchrotron for beamtime and for technical assistance.

References

1 Ball P.J. and R.J. Gilkes. 1987. The Mount Saddleback bauxite deposit, Southwestern Australia. *Chemical Geology* 60: 215-225 215.

2 Mehra, O. and P. Jackson. 1960. Iron oxide removal from soils and clays in a dithionite-citrate-bicarbonate system buffered with sodium bicarbonate. *Clays Clay Miner*. 7: 317-327

3 Zwingmann N., A.J. Jones, S. Dye, P.M. Swash and R.J. Gilkes. 2009. A method to concentrate boehmite in bauxite by dissolution of gibbsite and iron oxides. *Hydrometallurgy* 97: 80-85.

4 Brown, G. and G.W. Brindley. 1980. X-ray diffraction procedures for clay mineral identification, pp. 305-359. In G.W. Brindley and G. Brown, eds. Crystal Structures of Clay Minerals and Their X-ray Identification. Mineralogical Society, London.

5 Anand R.R. and R.J. Gilkes. 1987. Iron oxides in lateritic soils from Western Australia. *Journal of Soil Science* 38: 607-622.

6 Singh, B. and R.J. Gilkes. 1992. Properties of soil kaolinite from south-western Australia. *Journal of Soil Science* 43: 645-668.